

Complete fusion of $^{16,18}\text{O}$ with ^{27}Al and ^{nat}Si

R. Rascher, W. F. J. Müller, and K. P. Lieb

Institut für Kernphysik der Universität zu Köln, 5 Köln 41, Germany

(Received 22 January 1979)

Total fusion-evaporation cross sections for the systems $^{27}\text{Al} + ^{16,18}\text{O}$ and $^{nat}\text{Si} + ^{16,18}\text{O}$ have been measured in the energy range $34 \text{ MeV} \leq E_{\text{lab}} \leq 81 \text{ MeV}$ by detecting the evaporation residues in a time-of-flight spectrometer. The fusion cross sections for all systems were found to saturate at 1150–1200 mb. Fusion barriers have been deduced with the parametrization of Glas and Mosel. The data have also been discussed in terms of the Bass model.

[NUCLEAR REACTIONS $^{16,18}\text{O} + ^{27}\text{Al}$, $^{16,18}\text{O} + ^{nat}\text{Si}$; $E_{\text{lab}} = 34 - 81 \text{ MeV}$; measured σ_{fusion} ; deduced fusion barriers.]

I. INTRODUCTION

Previous studies on heavy-ion-induced fusion reactions have revealed a number of interesting phenomena.¹ For most lighter systems studied, the behavior of the total fusion-evaporation cross section (σ_F) as a function of bombarding energy can be divided into two regions. Shortly above the barrier, σ_F rises approximately linearly with $1/E_{\text{c.m.}}$ and may conveniently be parametrized by the radius R_B and height V_B of the fusion barrier at zero angular momentum. These parameters of the fusion barrier are to be compared with the radius R_0 and height V_0 of the s -wave interaction barrier deduced from elastic scattering data or total cross section measurements. Whereas the barrier heights V_B and V_0 turn out to be close to each other, considerable deviations between the radii R_B and R_0 have been encountered in some instances, among them $^{27}\text{Al} + ^{16,18}\text{O}$ (Ref. 2). The linear increase of the fusion cross section versus $1/E_{\text{c.m.}}$ proceeds up to the onset of deep-inelastic reaction channels, above which energy σ_F increases less strongly or even may reach a maximum value and decrease at higher energies. From a survey of the measured maximum values σ_F^{max} for different target-projectile combinations near the doubly magic $^{16}\text{O} + ^{16}\text{O}$ case, Sperr *et al.*³ suggested that the maximum fusion cross section may show shell effects.

Apart from the determination of the fusion barrier and the search for the existence of a maximum in the fusion cross section, a study of the system $^{28}\text{Si} + ^{16}\text{O}$ appeared challenging for several other reasons. In the fusion of "light" heavy ions with possible α -cluster structure such as $^{12}\text{C} + ^{12}\text{C}$ or $^{16}\text{O} + ^{12}\text{C}$, pronounced oscillations have been observed which, however, did not occur in the heavier systems^{4,5} $^{24}\text{Mg} + ^{16}\text{O}$ and $^{40}\text{Ca} + ^{16}\text{O}$. The $d_{5/2}$ subshell closure of ^{28}Si makes this target particularly interesting, also in view of the recent ob-

servation of resonances in the elastic scattering cross section⁶ of ^{16}O ions on ^{28}Si .

In a previous paper, Dauk *et al.*⁷ reported on the determination of σ_F for the systems ^{27}Al , $^{28}\text{Si} + ^{16}\text{O}$ from an analysis of the absolute γ -ray intensities of the evaporation residues. An essential short-coming of this method is the direct population of ground states of stable or long-lived evaporation residues. This fraction which escapes detection has been estimated to account for up to 30% of the fusion cross section near the barrier. It thus seemed worthwhile to check the previous results by applying an experimental technique in which the residual nuclei are directly detected with high efficiency in a time-of-flight spectrometer.

The choice of ^{18}O as the second projectile was motivated by the following consideration: Tabor *et al.*⁴ studied the fusion of $^{16,18}\text{O}$ ions with ^{24}Mg and observed rather different fusion barriers of the two systems. Even larger differences in the shape and magnitude of the fusion cross section have been measured for $^{12}\text{C} + ^{16,18}\text{O}$: The fusion cross section for $^{12}\text{C} + ^{18}\text{O}$ increases smoothly up to 1200 mb, whereas it oscillates in the former system and reaches a maximum value of only 940 mb.⁸

The present measurements of the fusion-evaporation cross sections for ^{27}Al , $^{28}\text{Si} + ^{16,18}\text{O}$ have been performed by means of a new heavy-ion time-of-flight spectrometer set up at the tandem accelerator of the University of Cologne. Its performances, as well as data taking and analysis, will be shortly described in Sec. II, whereas the results will be presented and discussed in Secs. III and IV.

II. EXPERIMENTAL PROCEDURE AND ANALYSIS

A. The spectrometer

The evaporation residues produced in a heavy-ion fusion reaction travel at low speed into a rather

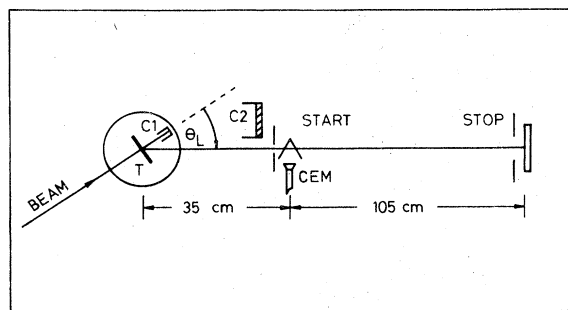


FIG. 1 Schematic setup of the time-of-flight spectrometer. T =target, $C1$, $C2$ =Faraday cups, CEM=channel electron multiplier.

narrow cone around the beam axis. Therefore the time-of-flight spectrometer (TFS) was designed according to the following conditions:

(1) An angular range from about 3° up to 30° should be scanned with the position of the TFS changed under vacuum.

(2) A mass-identification system was to be used with good energy resolution, very low-energy cut-off, moderate time resolution, and high efficiency.

Such apparatus has been previously described, e.g., by Pfeffer *et al.*⁹

The TFS (see Fig. 1) is made of a fixed sliding seal chamber containing the beam entrance slits, the target holder with six targets and the beam stop $C1$, and the flight chamber. The latter is mounted to a correlation table and can be moved under vacuum between 0° and 50° . The flight path between the start and stop detector is 105 cm long.

All reaction fragments produced by the 3–50 nA ^{16}O and ^{18}O beams reach the stop detector by passing through two 5–10 $\mu\text{g}/\text{cm}^2$ thin carbon foils which are mounted at 60° to the axis of the flight path. The ions produce secondary electrons which are accelerated by 1 kV voltage to the entrance of the channel electron multiplier (CEM),⁹ where they form the start signal. Electrons from the target are shielded from the CEM by permanent magnets mounted at the exit of the target chamber and by the two carbon foils. The stop detector was a 100 μm thick totally depleted silicon surface barrier detector which was cooled to -5°C and overbiased by a factor of 2.5 to improve the energy resolution for low-energy evaporation residues. The improvement was checked in a control experiment at the Bochum dynamitron accelerator. A beam of 15 MeV ^{28}Si ions was scattered from a thin Au foil; the energy resolution for the scattered ions was found to decrease from 330 to 260 keV full width at half maximum (FWHM) when overbiasing the detector.

A collimator of 12 mm in diameter in front of

the Si detector defined the solid angle of 0.06 msr accepted by the TFS. A second collimator with a larger solid angle in front of the carbon foils of the start detector was carefully matched to the first one so that small angle scattering of the evaporation residues was compensated for. It was found experimentally and verified by a rough calculation¹⁰ that about 8% of the fusion products escape detection if, because of small angle scattering, the two solid angles are geometrically equal.

The time resolution of the apparatus achieved with conventional electronics varied between 0.7 and 1.1 ns FWHM. The time spread affects the mass resolution

$$\Delta m/m = [(\Delta E/E)^2 + (2\Delta t/t)^2]^{1/2}$$

by about 20–66% for heavy recoils ($A=40$) in the energy range between 7 MeV $\leq E_R \leq 27$ MeV.

Normalization of the angular distributions was done in the following way: For $\theta \geq 9^\circ$, the beam was dumped into the Faraday cup $C1$, which had a diameter of only 0.5 cm and was positioned 3.5 cm behind the target. Self-supporting targets of 100 $\mu\text{g}/\text{cm}^2$ Si or Al backed by a 2 $\mu\text{g}/\text{cm}^2$ Au layer were used. The Au/Si and Au/Al ratios were determined from Rutherford scattering at 32 MeV beam energy and $\theta=16^\circ$. All excitation functions taken at $\theta=8^\circ$ and those parts of the angular distributions with $\theta \geq 9^\circ$ were then normalized to Rutherford scattering from the Au layer.

For $\theta < 9^\circ$, the beam was stopped in the cup $C2$, which was mounted in front of the start detector (see Fig. 1). When rotating the TFS, the beam hits different positions of $C2$. As the angular distributions at forward angles were normalized with respect to the total beam charge accumulated, a highly reliable relative measurement of this quantity was required. This was achieved by covering the cup with two permanent magnets of 500 G field strength in which secondary electrons are trapped. The accuracy of the beam integration was checked to be better than 1%. For measurements at forward angles, 50 $\mu\text{g}/\text{cm}^2$ thin self-supporting targets without Au backings were used. The two parts of each angular distribution were then interconnected at 9° .

We used silicon targets of natural composition (^{28}Si : 92.2%) as we did not succeed to manufacture thin self-supporting ^{28}Si targets free of oxygen. Fusion-evaporation products from the ^{16}O contaminant are not fully separated around mass 30–32 from the evaporation residues of the target. Furthermore, the elastic scattering peaks overlap at forward angles and thus introduce an uncertainty into the normalization.

As Rutherford scattering served for the overall

normalization of the data, the angle of the TFS with respect to the beam axis had to be adjusted with high accuracy. For that purpose, a pair of Si detectors was arranged in the flight chamber symmetrically at 20° to the axis of the TFS. The spectrometer was set into the zero position and the count rates of oxygen ions scattered from a 0.2 mm wide, $50 \mu\text{g}/\text{cm}^2$ thick Au target were recorded in both detectors.

B. Data analysis

Data were processed on-line in a PDP 11/20 computer. For each reaction product, its recoil energy (E), flight time (T), and channeltron amplitude (C) were stored in event-by-event mode on magnetic tape for off-line analysis. An event was accepted whenever an energy signal was present, even without a time signal. In this way, the efficiency of the start detector was tested on-line. The total count rate in the E detector was below 1.3 kHz; the total count rate at the computer was kept below 200 Hz by digitally reducing the elastic peak(s) at forward angles by a factor of 2^n , $n \leq 5$. The C signal was used to monitor the performance of the channeltron at high count rates.

The data were transformed off-line into an energy versus mass matrix by means of the program MANTO.¹¹ An example which refers to the system $\text{Si} + {}^{18}\text{O}$ at $\theta = 9^\circ$ and $E_{\text{lab}} = 50 \text{ MeV}$ is shown in Fig. 2. Also shown are the projection of the full matrix onto the mass axis and the projection of the encircled fusion region and the elastic lines (Au, Si, O, C) onto the energy axis. Although some oxidation of the Si target and carbon buildup were unavoidable,

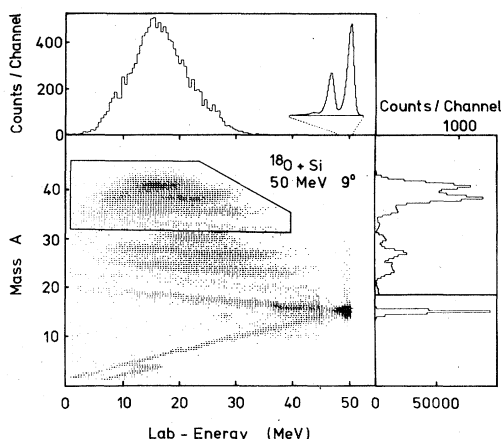


FIG. 2. Mass versus energy matrix of the reaction products taken for the system $\text{natSi} + {}^{18}\text{O}$ at 50 MeV beam energy and $\theta_{\text{lab}} = 9^\circ$. The upper part shows the projection of the encircled region of the matrix onto the energy axis; the insert shows, with enlarged energy scale, the peaks from elastic scattering. The projection onto the mass axis is displayed on the right-hand side.

the evaporation residues of these contaminants were clearly separated in all spectra. Note also the low cutoff energy of the fusion spectrum at about 2 MeV. The diagonal line connecting the elastic peak(s) with the origin contains those few events in which oxygen ions have been elastically scattered from the aperture of the stop detector. A total of about 10^4 fusion events were accumulated in each spectrum. The error of $d\sigma_F/d\theta$ was typically 3%, including statistics, an uncertainty of $\Delta\theta = 0.08^\circ$ in the direction of the TFS which affects the normalization to Rutherford scattering, an uncertainty of 1% in the target thickness relative to Au, and an error of 1% in the relative current integration.

The projected mass spectrum of the evaporation residues shown in Fig. 2 clearly reveals several peaks associated with the evaporation of 0–3 α particles (and up to two nucleons) from the initial compound system.⁷ The angular distributions $d\sigma/d\theta$ of the four mass components for ${}^{27}\text{Al} + {}^{18}\text{O}$ at 70 MeV are shown in Fig. 3. At this energy at which

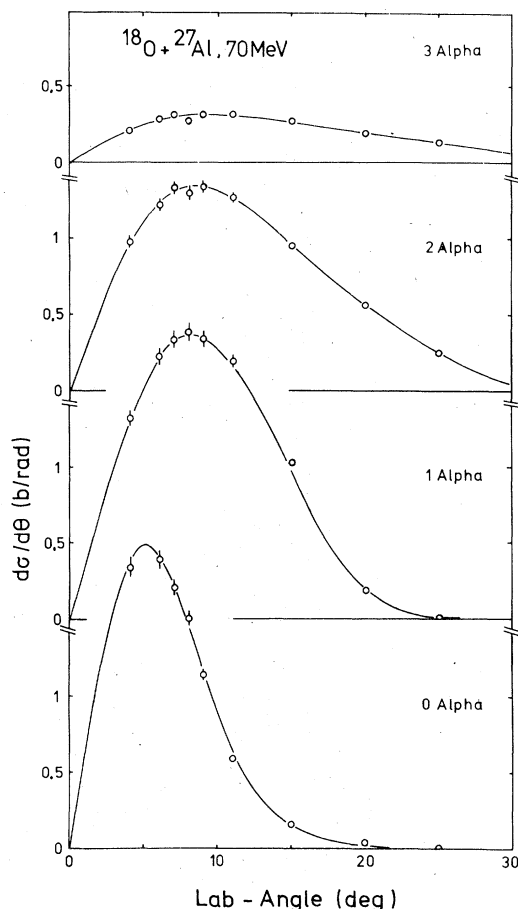


FIG. 3. Angular distributions of the evaporation residues grouped with respect to the emission of 0–3 α particles, for the system ${}^{27}\text{Al} + {}^{18}\text{O}$ at 70 MeV.

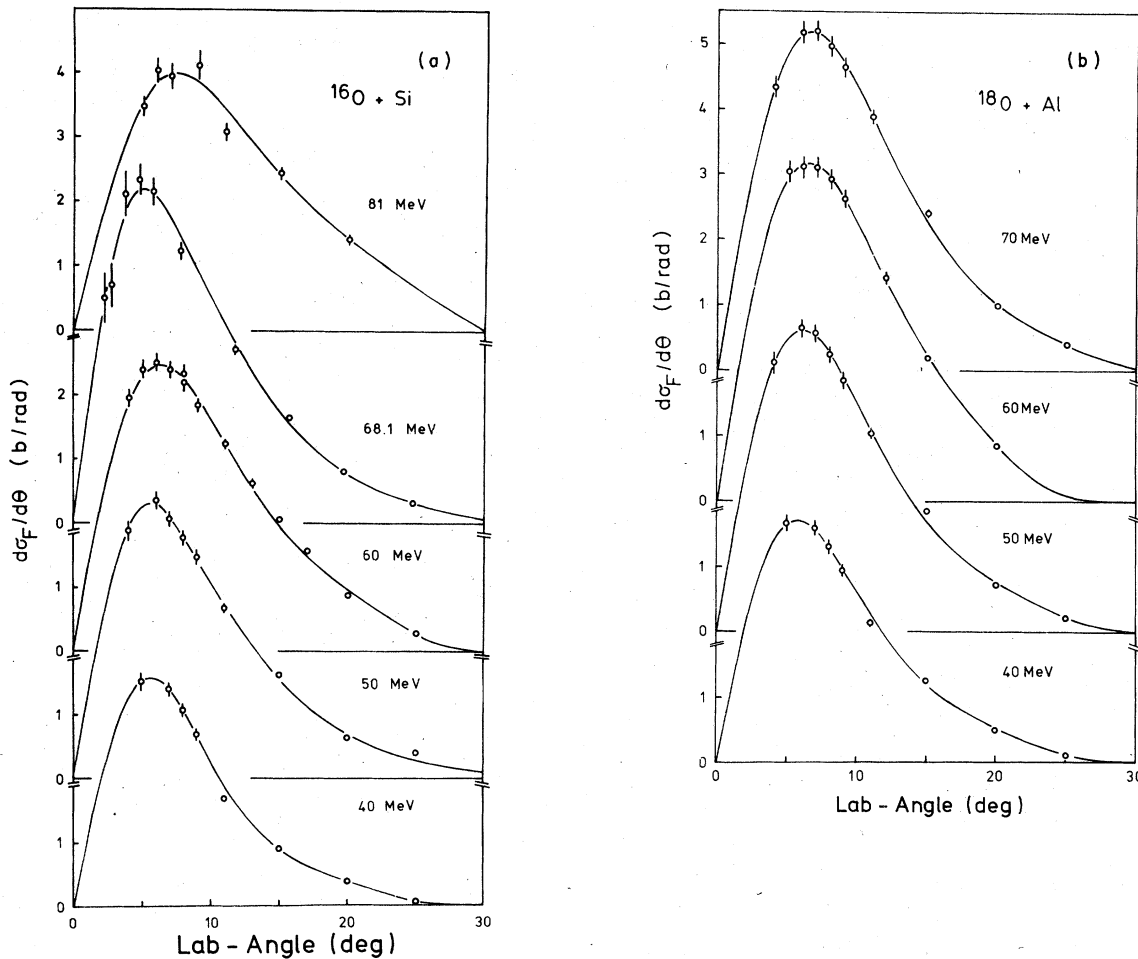


FIG. 4. (a) Measured angular distributions of all fusion-evaporation residues produced in the reaction $^{\text{nat}}\text{Si} + ^{16}\text{O}$. The fits are discussed in the text. (b) Same as in Fig. 3(a) for the reaction $^{27}\text{Al} + ^{18}\text{O}$.

σ_F saturates, the $(3\alpha + \text{nucleon})$ channel contributes by about 11% to the total fusion cross section. This mass component may also contain an appreciable fraction of targetlike fragments from transfer and deep-inelastic reactions. Several authors^{12,13} have studied the mass, energy, and angular momentum transfer of these reactions for the system $^{27}\text{Al} + ^{16}\text{O}$ at 65–100 MeV beam energy. The dominant transfer channel is the $(^{16}\text{O}, ^{12}\text{C})$ reaction at an optimal Q value of 25 MeV, followed by the evaporation of up to two nucleons. If we transform the differential cross section $d^2\sigma/d\Omega dE$ measured for the light fragment ^{12}C into the system of the targetlike fragment (i.e., ^{31}P), we find at 70 MeV beam energy an average recoil energy of 10 MeV and a broad angular distribution which overlaps with the fusion-evaporation products. For the system $^{27}\text{Al} + ^{18}\text{O}$, the estimated fraction of products of transfer reactions with $A \approx 30, 31$ is not larger than 30 mb, i.e., about 2% of the fusion cross section.

III. RESULTS

Angular distributions of the evaporation residues have been taken in about 10 MeV intervals between 40 and 81 MeV. Part of them are shown in Fig. 4 for the systems $^{27}\text{Al} + ^{18}\text{O}$ and $^{\text{nat}}\text{Si} + ^{16}\text{O}$. The only feature of these distributions is the broad maximum of $d\sigma_F/d\theta$ which moves from about 6° at 40 MeV to 8° at 70 MeV beam energy. This change, as well as the rising tail at $\theta > 9^\circ$, reflects the increasing number of α particles whose evaporation is favored by Q values (see also Fig. 3).

A parametrization of the angular distribution convenient for integration was found to be

$$\frac{d\sigma_F}{d\Omega} \propto \exp[-(\theta/\theta_0)^2 + a_4(\theta/\theta_0)^4 + a_6(\theta/\theta_0)^6],$$

where the fitted parameters are $\theta_0 \sim 7^\circ$, a_4 and a_6 with $|a_4| \ll 1$ and $|a_6| \ll 1$. As the angular distributions change so little with energy, the other values

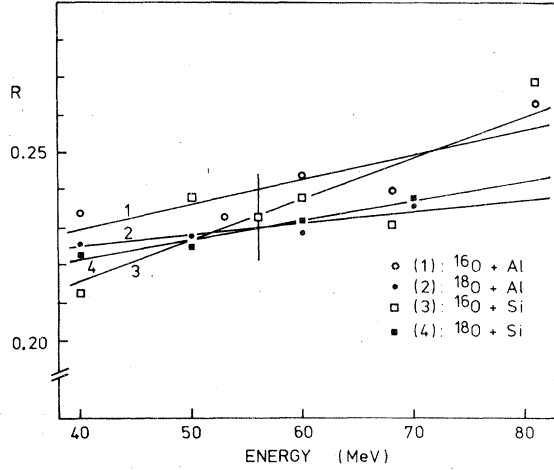


FIG. 5. Ratio R between the angle-integrated fusion cross section σ_F and the differential cross section $d\sigma_F/d\theta$ at $\theta_{\text{lab}} = 8^\circ$.

of σ_F have been obtained from excitation functions measured at $\theta = 8^\circ$ from 34–81 MeV for ^{16}O projectiles and from 34–72 MeV for ^{18}O projectiles, respectively. The differential cross sections $(d\sigma_F/d\Omega)_{8^\circ}$ were converted into total fusion cross sections σ_F by linearly interpolating the measured ratios $R = \sigma_F/(d\sigma_F/d\Omega)_{8^\circ}$, shown in Fig. 5. The estimated errors of σ_F are 4–5%.

The measured fusion-evaporation cross sections are listed in Table I and plotted in Fig. 6 versus $1/E_{\text{c.m.}}$. Excellent agreement of our work with the results of Eisen *et al.*² and Back *et al.*¹⁴ was found for the system $^{27}\text{Al} + ^{16}\text{O}$, which served to test the reliability of our TFS. We recall that Back *et al.*¹⁴ have obtained their results by means of a time-of-flight spectrometer with mass identification, whereas Eisen *et al.*² identified the nuclear charges of the reaction fragments in ΔE - E telescopes. In Fig. 7, all values of σ_F for this system obtained from particle spectra are compared to those found from γ -ray spectroscopy.⁷ The larger error bars of the γ -spectroscopic data⁷ reflect mostly the accumulated statistical errors of the intensities of the many γ -ray transitions. The incorrect saturation of these data at $1/E_{\text{c.m.}} \approx 0.035 \text{ MeV}^{-1}$ is probably due to the neglect of the evaporation residues with $A \leq 34$, i.e., the 3α , $2\alpha p$, and $2\alpha\gamma$ channels. The γ -spectroscopic data are also systematically too low by about 20%; this discrepancy is partly the effect of ground state populations.⁷

All excitation functions shown in Fig. 6 follow approximately a smooth $1/E_{\text{c.m.}}$ dependence and saturate at $\sigma_F^{\text{max}} = 1140$ –1200 mb. None of the curves shows fluctuations larger in amplitude than the typical error of 4% of the individual data points. However, the 2 MeV interval of the excitation

TABLE I. Measured fusion-evaporation cross sections (in mb). Angular distributions are marked with "A."

E_{lab} (MeV)	$^{27}\text{Al} + ^{16}\text{O}$	$^{27}\text{Al} + ^{18}\text{O}$	$\text{Si} + ^{16}\text{O}$	$\text{Si} + ^{18}\text{O}$
34.0	563(27)	...	404(29)	439(20)
36.0	609(25)	604(20)	481(26)	527(22)
38.0	716(30)	676(22)	556(31)	603(26)
40.0	771(21) A	747(23) A	659(22) A	650(21) A
42.0	812(30)	813(25)	730(30)	740(26)
44.0	...	862(28)	...	787(29)
46.0	926(31)	898(30)	870(32)	826(27)
48.0	...	928(30)	...	870(30)
50.0	1010(26) A	980(30) A	907(20) A	919(22) A
53.0	1015(36) A
54.0	1043(36)	1059(33)	...	983(32)
56.0	1097(38)	1104(34)	1064(37)	1011(33)
56.1	1051(36) A	...
58.0	1134(37)	1108(33)	1070(38)	1029(30)
60.0	1160(20) A	1136(35) A	1072(50)	1103(25) A
62.0	1129(39)	1153(35)	1130(34)	1095(32)
64.0	1162(38)	1187(37)	1139(36)	1115(31)
66.0	1135(38)	1197(37)	1142(37)	1140(38)
68.0	1164(36)	1179(37)	1164(38)	1151(37)
68.1	1160(24)	...	1187(29) A	...
70.0	1182(37)	1185(35) A	1203(38)	1109(25) A
72.0	...	1216(38)	1201(37)	1144(39)
76.0	1251(48)
78.0	1297(41)	...
81.0	1120(40) A	...	1070(40) A	...

functions may have been too large to resolve possible finer structures. We finally note that our data for the system $^{27}\text{Al} + ^{16}\text{O}$ favor a smoother behavior of σ_F near the saturation point than the abrupt change suggested by Back *et al.*¹⁴

IV. DISCUSSION

The measured fusion-evaporation cross sections have been compared with the models of Glas and Mosel¹⁵ and Bass.¹⁶ In the approximation of Glas and Mosel,¹⁵ all partial waves up to the (energy dependent) critical value

$$l_c = R_c [2\mu(E_{\text{c.m.}} - V_c)]^{1/2} / \hbar$$

contribute to fusion, once the fusion barrier is overcome. The reduced critical radius $r_c = R_c / (A_1^{1/3} + A_2^{1/3})$ is of the order of 1 fm,¹ and V_c denotes the nuclear potential at $r = R_c$. In the vicinity of the barrier, σ_F is determined by the parameters V_B , R_B , and the curvature $\hbar\omega$ of the barrier. These assumptions lead to a nearly linear dependence of σ_F versus $1/E_{\text{c.m.}}$ in the low-energy domain ($E_{\text{c.m.}} \gtrsim V_B$)

$$\sigma_F \approx \pi R_B^2 (1 - V_B/E_{\text{c.m.}}),$$

as well as in the high-energy domain ($E_{\text{c.m.}} \gg V_B$)

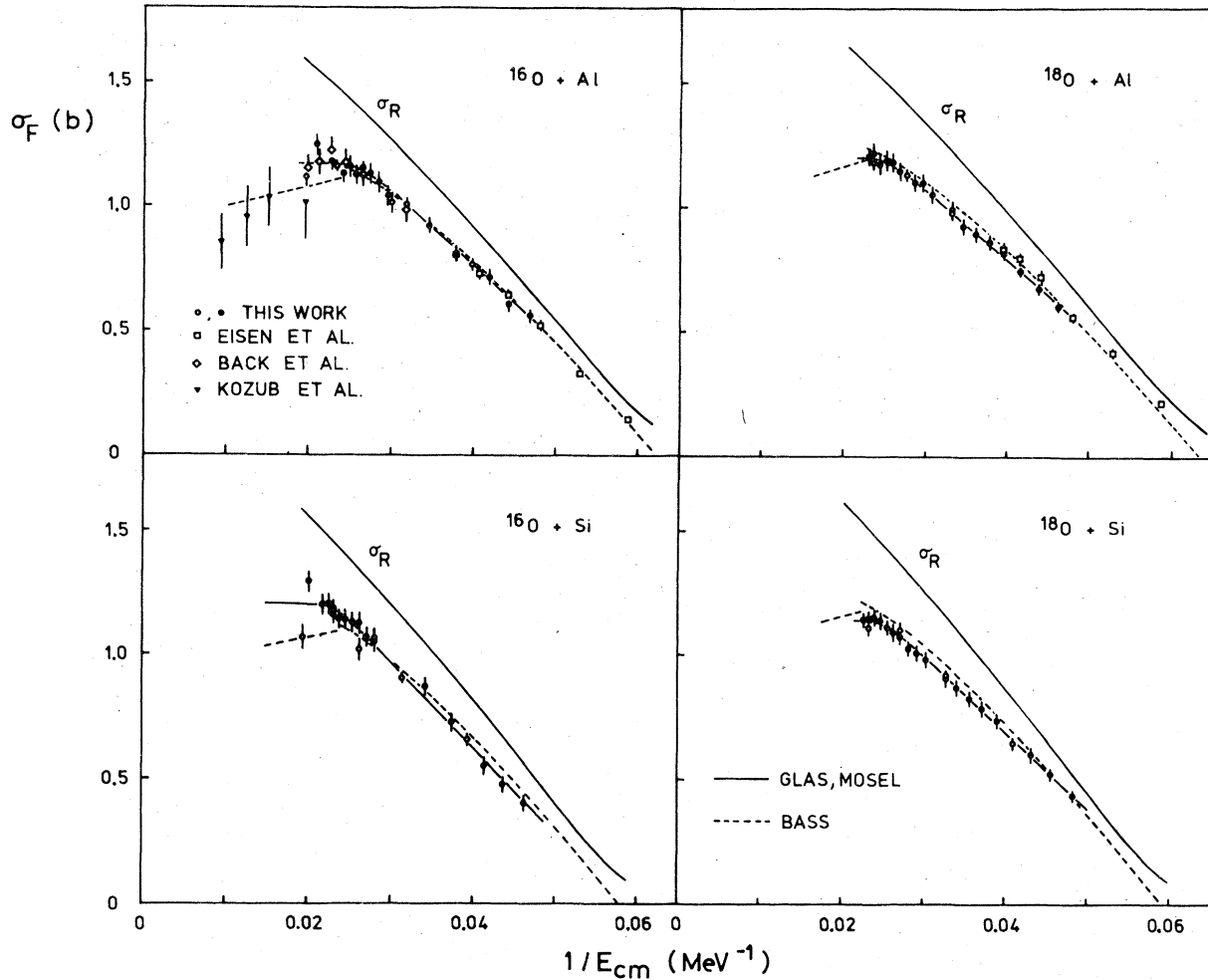


FIG. 6. Measured fusion-evaporation cross sections for ^{27}Al , $^{\text{nat}}\text{Si} + ^{16,18}\text{O}$. Also given are the experimental results of Refs. 2, 14, and 17. The open circles of the present work refer to data which have been integrated over full angular distributions. The Glas-Mosel parametrization and the Bass model, as well as the reaction cross sections σ_R , are discussed in the text.

$$\sigma_F \approx \pi R_c^2 (1 - V_c/E_{\text{c.m.}}).$$

Owing to the energy limitation of the accelerator, only data in the low-energy region have been gathered and thus only the barrier parameters R_B and V_B can be deduced with good accuracy. The critical parameters R_c and V_c influence to some extent σ_F near the saturation point. For all systems except $^{27}\text{Al} + ^{16}\text{O}$, where some high-energy points¹⁷ have been measured (see Fig. 7), we set $V_c = 0$, following Ref. 4, and adjusted R_B , V_B , and R_c individually to fit the data. As in Ref. 4, a barrier width of $\hbar\omega = 5$ MeV was adopted. The fits are shown in Figs. 6 and 7, and the deduced barrier parameters are listed in Table II, which also summarizes the results of some other oxygen induced fusion reactions analyzed in the same way.

Several points are noteworthy: Let us first dis-

cuss the dependence of R_B and V_B on the energy range used in the fit and the high-energy parameters V_c and R_c . For the systems $^{27}\text{Al} + ^{16,18}\text{O}$, Eisen *et al.*² determined R_B and V_B from data below 42 MeV beam energy, whereas the measurements of Back *et al.*¹⁴ and of the present work reach up to the saturation point around $E_{\text{lab}} = 70$ MeV. For the fusion barrier of $^{27}\text{Al} + ^{16}\text{O}$, good agreement among the three sets of parameters is found, but we note a difference of $\Delta R_B = 0.48 \pm 0.25$ fm and $\Delta V_B = 0.9 \pm 0.4$ MeV for the system $^{27}\text{Al} + ^{18}\text{O}$. The influence of R_c and V_c on the fusion parameters can be studied for the system $^{27}\text{Al} + ^{16}\text{O}$ making use of the high-energy data by Kozub *et al.*¹⁷ A fit to all low- and high-energy data shown in Fig. 7 yields $r_c = 0.99 \pm 0.06$ fm and $V_c = -11 \pm 6$ MeV. If we disregarded the high-energy data and set $V_c = 0$, we obtain $r_c = 1.1$ fm. However, these values are

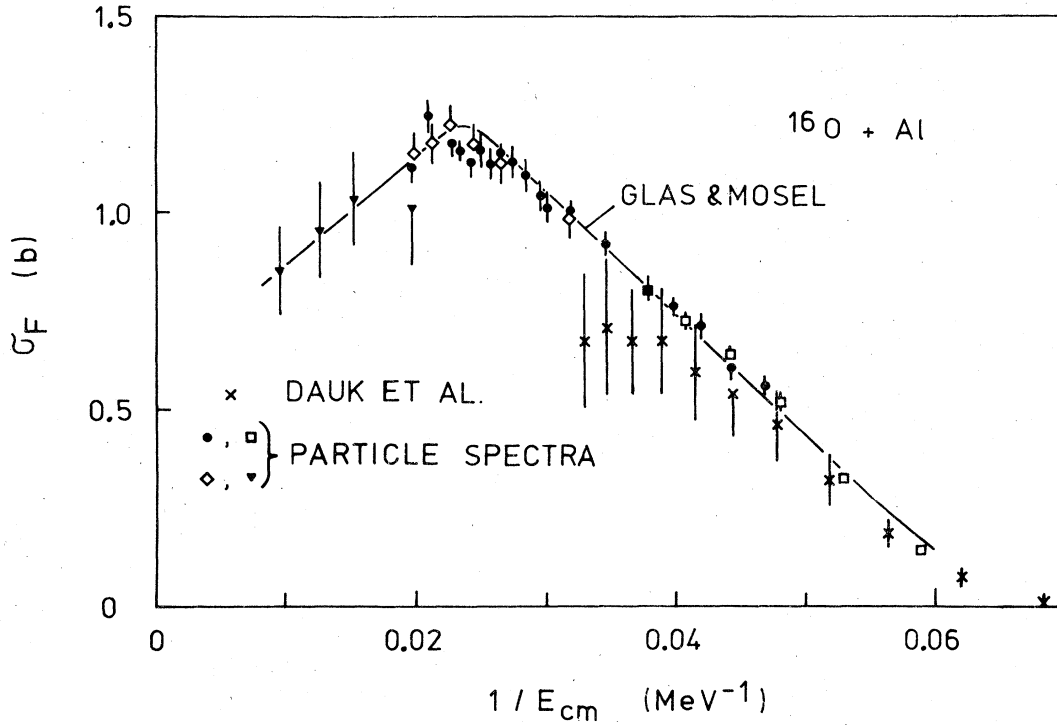


FIG. 7. Comparison of all fusion-evaporation cross sections for the system $^{27}\text{Al} + ^{16}\text{O}$ obtained from particle work with the results of the γ -spectroscopic study of Dauk *et al.*, (Ref. 7). The curve labeled "Glas and Mosel" is a fit to all data from particle spectra: $V_B = 15.75(8)$ MeV, $R_B = 8.05(5)$ fm, $V_C = -11(6)$ MeV, $R_C = 5.5(3)$ fm, and $\hbar\omega = 5$ MeV.

TABLE II. Deduced fusion barriers in the parametrization of Glas and Mosel (Ref. 15) compared with the values obtained from the proximity potentials of Bass (Ref. 16) and Blocki *et al.* (Ref. 19).

Reaction	Experiment				Bass (Ref. 16)		Blocki <i>et al.</i> (Ref. 19)		Ref.
	r_B (fm)	r_c (fm)	R_B (fm)	V_B (fm)	R_B	V_B	R_B	V_B	
$^{16}\text{O} + ^{12}\text{C}$	1.57(3)	...	7.55(14)	7.7(1)	7.9	8.0	7.5	8.3	3
$^{18}\text{O} + ^{12}\text{C}$	1.60(2)	1.04 ^b	7.86(10)	7.5(1)	8.1	7.8	7.7	8.1	3
$^{16}\text{O} + ^{16}\text{O}$	1.46	...	7.36	11.5	8.1	10.4	7.7	10.9	26
	1.63(2)	1.1(3)	8.2(11)	10.9(11)					25
$^{16}\text{O} + ^{24}\text{Mg}$	1.57(5)	1.08	8.48(25)	16.0(5)	8.6	15.0	7.9	15.8	4
$^{18}\text{O} + ^{24}\text{Mg}$	1.42(4)	1.15	7.82(23)	14.8(5)	8.7	14.7	8.1	15.4	4
$^{16}\text{O} + ^{26}\text{Mg}$	1.59(5)	0.97 ^b	8.72(26)	16.6(5)	8.6	14.8	8.1	15.5	4
$^{16}\text{O} + ^{27}\text{Al}$	1.46(1)	0.99(6)	8.05(5)	15.8(1)	8.6	16.0	8.1	16.8	c
	1.43(2)	1.11	7.91(11)	15.4(3)					d
	1.44(4)	0.79(14)	7.95(22)	16.1(5)					14
	1.48(3)	...	8.19(17)	15.7(1)					2
$^{18}\text{O} + ^{27}\text{Al}$	1.41(2)	1.10	7.95(10)	15.0(2)	8.8	15.7	8.3	16.5	e
	1.48(4)	...	8.34(22)	15.6(2)					2
	1.39(2)	1.10	7.84(16)	14.7(3)					d
$^{16}\text{O} + ^{28}\text{Si}$	1.44(2) ^a	1.11	7.98(10)	17.2(3)	8.6	17.2	8.1	18.1	d
$^{18}\text{O} + ^{28}\text{Si}$	1.38(2) ^a	1.07	7.84(10)	16.0(3)	8.8	16.9	8.3	17.8	d
$^{16}\text{O} + ^{40}\text{Ca}$	1.52	1.02	9.03	23.7	8.9	23.7	8.4	25.0	5
$^{16}\text{O} + ^{148}\text{Nd}$	1.25(3)	...	9.76(23)	57.8(2)	10.8	59.5	10.4	61.6	18
$^{18}\text{O} + ^{148}\text{Nd}$	1.17(3)	...	9.25(24)	58.3(2)	11.0	58.5	10.6	60.7	18

^a Corrected for isotope composition of target.

^b $V_C = -10$ MeV (Refs. 3 and 27).

^c Fitted to all data of Refs. 2, 14, and 17 and present work; $V_C = -11(6)$ MeV.

^d Present work.

^e Fitted to data of Ref. 2 and present work.

at variance with a fit proposed by Back *et al.*¹⁴ ($V_c = -46$ MeV, $r_c = 0.79 \pm 0.01$ fm) and demonstrate the need of precise high-energy fusion cross sections.

Next we compare the fusion barriers for ^{16}O and ^{18}O projectiles for different targets. Accurate values of R_B and V_B have been evaluated for the targets ^{12}C (Refs. 3 and 8), ^{24}Mg (Ref. 4), ^{27}Al , ^{28}Si , and ^{148}Nd (Ref. 18). It is evident that the reduced barrier radii $r_B = R_B/(A_1^{1/3} + A_2^{1/3})$ for fusion with ^{18}O are smaller than for fusion with ^{16}O ; R_B thus does not follow a simple $A^{1/3}$ trend. (The fusion radii of $^{16,18}\text{O}$ on ^{12}C do not seem to show this difference. One should, however, remember the strong resonancelike structure⁸ in the fusion of ^{12}C with ^{16}O which may have affected the deduced barrier parameters.) As no systematic study of the other reaction channels has been undertaken we cannot offer a quantitative explanation of this difference at present, but we suggest that few-nucleon transfer reactions and projectile excitation are more important in the case of ^{18}O induced reactions and reduce the fraction of the total reaction cross section going into fusion.

Whereas Glas and Mosel¹⁵ offer a ready parametrization of σ_F for the individual systems studied, one may compare σ_F , R_B , and V_B directly with the predictions based on an overall nucleus-nucleus potential. Blocki *et al.*,¹⁹ Bass,¹⁶ and Birkelund and Huizenga²⁰ have recently discussed the proximity potential in connection with heavy-ion fusion. In this approximation, the nuclear potential V_N factorizes as $V_N = 4\pi\gamma\Phi(\xi)b\bar{C}$, where $\xi = r - C_1 - C_2$ is the distance between the two nuclear surfaces, and $C_i = R_i[1 - (b/R_i)^2]$, $b = 1$ fm. The universal function $\Phi(\xi)$ relates to the energy density of two infinite, parallel "sheets" of nuclear matter, and $\bar{C} = C_1C_2/(C_1 + C_2)$ accounts for the finite sizes of the colliding ions. Blocki *et al.*¹⁹ adjusted the coefficient γ of the surface energy from the mass formula; on the other hand, Bass¹⁶ normalized the expression $4\pi\gamma\Phi(\xi)$ to achieve an overall best fit to the fusion cross sections of many target-projectile combinations. For both potentials V_N , the parameters R_B and V_B were calculated and are given in the last columns of Table II. Although the small differences between ^{16}O and ^{18}O fusion radii are not reproduced, both potentials describe correctly the general trend with the target nucleus. It appears that the Bass model¹⁶ fits better the barrier height V_B , whereas the approach of Blocki *et al.*¹⁹ accounts better for the fusion radii R_B . As shown in Fig. 6, the Bass model reproduces well the measured fusion cross sections.

Also given in Fig. 6 is the total reaction cross section σ_R evaluated from optical model potentials. The two Woods-Saxon type potentials pro-

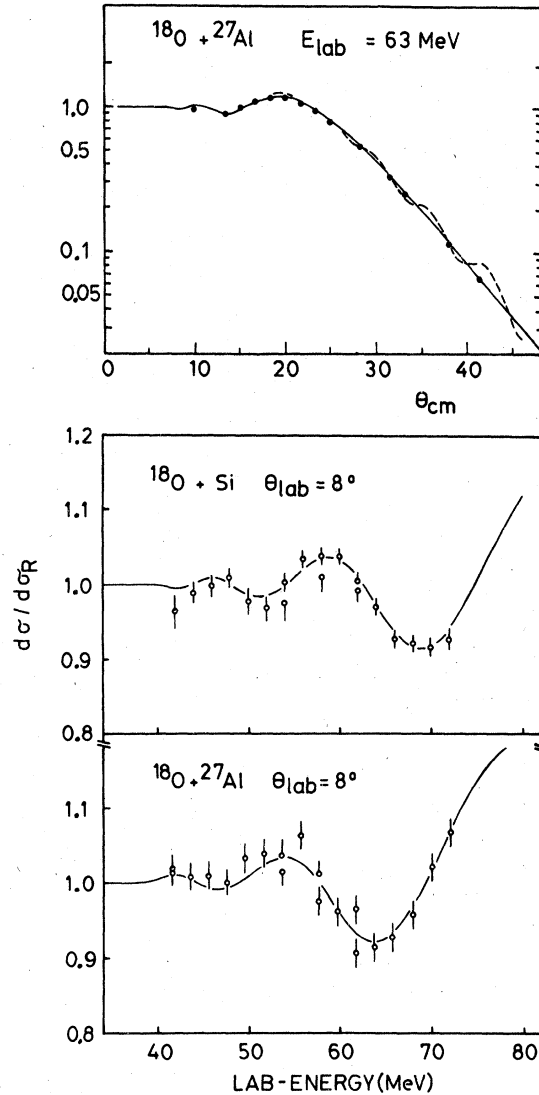


FIG. 8. Elastic scattering excitation functions (at $\theta_{lab} = 8^\circ$) and angular distribution (at $E_{lab} = 63$ MeV) for ^{27}Al , $^{nat}\text{Si} + ^{18}\text{O}$; the solid lines refer to a calculation with the optical model parameters of Cramer *et al.* (Ref. 21), the dashed line refers to the set of Eisen *et al.* (Ref. 2).

posed by Eisen *et al.*² for $^{27}\text{Al} + ^{16,18}\text{O}$ and by Cramer *et al.*²¹ for $^{28}\text{Si} + ^{16}\text{O}$ have been considered assuming a $(A_1^{1/3} + A_2^{1/3})$ scaling for all radii. As illustrated in Fig. 8, the shallow potential of Cramer *et al.*²¹ fits our elastic scattering cross sections better than the deep potential of Eisen *et al.*² Nonetheless, the reaction cross sections calculated with both potentials agree to within 2%. On the other hand, Satchler²² has pointed out that a folding potential, which fits the $^{28}\text{Si} + ^{16}\text{O}$ elastic scattering data equally well, yields a 10–20% higher reaction cross section.

It has been customary to compare the parameters R_B and V_B of the fusion barrier to the corresponding (Rutherford) radius R_0 and height V_0 of the s-wave barrier of the nuclear-plus-Coulomb potential. Such a procedure is justified whenever R_0 and V_0 can be unambiguously determined from the elastic scattering data as suggested, e.g., by Bertin *et al.*²³ Recent investigations, e.g., by Wojciechowski²⁴ have demonstrated, however, that R_0 and the diffuseness are correlated to some extent; in the present case, R_0 varies by 0.5 fm for the two potentials mentioned above. It appears, therefore, that a consistent strategy in fitting the elastic scattering data and/or precise measurements of the total reaction cross section is required in order to allow a meaningful comparison of the barrier parameters for many projectiles and targets.

V. CONCLUSION

The design of a new time-of-flight spectrometer allowed us to measure with good accuracy the fusion-evaporation cross sections σ_F for the systems ^{27}Al , $^{28}\text{Si} + ^{16,18}\text{O}$. In all cases, σ_F was found to increase linearly with $1/E_{\text{c.m.}}$ up to $E_{\text{c.m.}} \approx 37$ MeV and merge smoothly to saturation values of $\sigma_F^{\text{max}} = 1140\text{--}1200$ mb. In the parametrization of Glas and Mosel,¹⁵ the radii R_B and heights V_B of the fusion barriers were deduced. As previously observed for ^{24}Mg and ^{148}Nd targets, the ^{18}O fusion

radii for ^{27}Al and ^{28}Si were found to be slightly smaller than the ^{16}O radii. The survey of reduced fusion barriers r_B for $^{16,18}\text{O}$ induced reactions presented in Table II shows a decrease from $r_B \approx 1.6$ fm for carbon to $r_B \approx 1.2$ fm for $A \approx 150$. Both the Bass model¹⁶ and the proximity potential of Blocki *et al.*¹⁹ reproduce this trend.

Owing to the lack of precise data at higher energies, the role of friction forces, which may be responsible for the saturation of σ_F , is still not well understood. An extension of the present measurements above the saturation point up to $E_{\text{c.m.}} \approx 100$ MeV thus appears very challenging, although it may become more and more difficult to separate the evaporation residues from the fragments of transfer and deep-inelastic reactions.

ACKNOWLEDGMENTS

The authors would like to thank Dr. Pfeffer, Dr. N. Wüst, and N. Möller for their interest in the initial stages of the work; F. J. Bergmeister, H. P. Hellmeister, A. Henriquez, and J. Panqueva for their help during the measurements; L. Fruh for his expert advice concerning the mechanical setup of the spectrometer; and H. Bohnhoff and his crew for the excellent working conditions of the accelerator. Stimulating discussion with Professor U. Mosel are appreciated. This work was supported by the German Bundesministerium für Forschung und Technologie.

- ¹H. H. Gutbrod, W. G. Winn, and M. Blann, Nucl. Phys. **A213**, 267 (1973); M. Lefort, J. Phys. (Paris) **37**, 5 (1976); J. P. Schiffer, in *Procédés du Colloque Franco-Japonais de Spectroscopie Nucleaire*, edited by Y. Shida (Institute for Nuclear Study, Tokyo, 1976), p. 176; U. Mosel, in *Proceedings of the International Conference on Nuclear Interactions*, Canberra, 1978.
- ²Y. Eisen, I. Tserruya, Y. Eyal, Z. Fraenkel, and M. Hillman, Nucl. Phys. **A291**, 459 (1977).
- ³P. Sperr *et al.*, Phys. Rev. Lett. **37**, 321 (1976).
- ⁴S. L. Tabor, D. F. Geesaman, W. Henning, D. G. Kovar, K. E. Rehm, and F. W. Prosser, Jr., Phys. Rev. C **17**, 2136 (1978).
- ⁵D. F. Geesaman *et al.*, Phys. Rev. C **18**, 284 (1978).
- ⁶P. Braun-Munzinger *et al.*, Phys. Rev. Lett. **38**, 944 (1977).
- ⁷J. Dauk, K. P. Lieb, and A. M. Kleinfeld, Nucl. Phys. **A241**, 170 (1975).
- ⁸P. Sperr *et al.*, Phys. Rev. Lett. **36**, 405 (1976).
- ⁹W. Pfeffer, B. Kohlmeyer, and W. F. W. Schneider, Nucl. Instrum. Methods **107**, 121 (1973).
- ¹⁰R. Rascher, doctoral thesis (Universitat zu Köln, 1979) (unpublished).
- ¹¹W. F. J. Müller, thesis (Universitat zu Köln, 1979) (unpublished).
- ¹²J. W. Harris, T. M. Cormier, D. F. Geesaman, L. L. Lee, Jr., R. L. McGrath, and J. P. Wurm, Phys. Rev. Lett. **38**, 1460 (1977).
- ¹³T. M. Cormier *et al.*, Phys. Rev. C **13**, 682 (1976).
- ¹⁴B. B. Back, R. R. Betts, C. Gaarde, J. S. Larsen, E. Michelsen, and Tai Kuang-Hsi, Nucl. Phys. **A285**, 317 (1977).
- ¹⁵D. Glas and U. Mosel, Nucl. Phys. **A237**, 429 (1975).
- ¹⁶R. Bass, Phys. Rev. Lett. **39**, 265 (1977).
- ¹⁷R. L. Kozub, N. H. Lu, J. M. Miller, D. Logan, T. W. Debiak, and L. Kowalski, Phys. Rev. C **11**, 1497 (1975).
- ¹⁸R. Broda, M. Ishihara, B. Herskind, H. Oeschler, S. Ogaza, and H. Ryde, Nucl. Phys. **A248**, 356 (1975).
- ¹⁹J. Blocki, J. Randrup, W. Swiatecki, and C. F. Tsang, Ann. Phys. (N. Y.) **105**, 427 (1977).
- ²⁰J. R. Birkelund and J. R. Huizenga, Phys. Rev. C **17**, 126 (1978).
- ²¹J. G. Cramer, R. M. DeVries, D. A. Goldberg, M. S. Zisman, and C. F. Maguire, Phys. Rev. C **14**, 2158 (1976).
- ²²G. R. Satchler, Nucl. Phys. **A279**, 493 (1977).
- ²³M. C. Bertin, S. L. Tabor, W. A. Watson, Y. Eisen, and G. Goldring, Nucl. Phys. **A167**, 216 (1971).
- ²⁴H. Wojciechowski, N. B. J. Tannous, R. J. Davis, D. Stanley, M. Galin, and F. Petrovich, Phys. Rev. C **17**, 2126 (1978).
- ²⁵I. Tserruya, Y. Eisen, D. Pelte, A. Gavron, H. Oeschler, D. Berndt, and H. L. Harney, Phys. Rev. C **18**, 1688 (1978).
- ²⁶V. K. C. Cheng, A. Little, H. C. Yuen, S. M. Lazarus, and S. S. Hanna (unpublished).
- ²⁷D. Horn, A. J. Ferguson, and O. Häusser, Nucl. Phys. **A311**, 238 (1978).